IJECBE (2025), **3**, **4**, 735–754
Received (25 June 2025) / Revised (22 December 2025)
Accepted (22 December 2025) / Published (30 December 2025)
https://doi.org/10.62146/ijecbe.v3i4.164
https://ijecbe.ui.ac.id
ISSN 3026-5258

International Journal of Electrical, Computer and Biomedical Engineering

RESEARCH ARTICLE

Design and Analysis of Hybrid Energy Storage in PV Systems to Handle Irradiance Fluctuations

Raisah Anni Ritonga[†] and Faiz Husnayain[*†‡]

†Department of Electrical Engineering, Faculty of Engineering, Universitas Indonesia, Depok, Indonesia
‡Research Center for Advanced Vehicles (RCAVe), Faculty of Engineering, Universitas Indonesia, Depok, Indonesia
*Corresponding author. Email: faiz.h@ui.ac.id

Abstract

The increasing demand for energy and the need to reduce carbon emissions have accelerated the adoption of photovoltaic (PV)-based power systems. However, PV output is inherently intermittent due to variations in solar irradiance, leading to power fluctuations. Energy storage systems are therefore required to balance the mismatch between generation and load. Conventional battery storage suffers from limited response speed and power density, making it less effective in handling rapid transients. In contrast, supercapacitors provide high power density and fast dynamic response but are constrained by low energy density. This paper proposes a hybrid energy storage system (HESS) that integrates batteries and supercapacitors, along with a power-sharing control strategy to optimize their operation. The proposed approach enables the battery to manage long-term energy requirements, while the supercapacitor mitigates short-term fluctuations. Simulation results demonstrate that the supercapacitor effectively compensates for sudden load variations, and the HESS maintains system stability under varying irradiance and load conditions. Furthermore, the results confirm faster dynamic response of the supercapacitor compared to the battery, while the battery state of charge (SOC) reflects its role in long-term energy balancing.

Keywords: Photovoltaic (PV), Battery, Supercapacitor, Hybrid Energy Storage System (HESS)

1. Introduction

Since the second industrial revolution, global energy generation has largely relied on fossil fuel combustion, contributing to a substantial increase in atmospheric CO_2

levels. Reports indicate that between 1970 and 2002, global CO_2 emissions rose by over 70% [1]. In Asia, rising per capita GDP, population growth, and expansion in the energy and transportation sectors have been identified as the major contributors to this trend [2]. In Indonesia, while land uses have historically been the dominant source of greenhouse gas (GHG) emissions, projections suggest that the energy sector will surpass it by 2026–2027 [3]. In response, Indonesia ratified the Paris Agreement in 2015 and committed to achieving net-zero emissions by 2060, with solar energy being a key pillar of its renewable energy strategy [3].

Photovoltaic (PV) systems offer a clean and sustainable energy source. However, their output is inherently intermittent due to variations in solar irradiance and ambient temperature [4]. To maintain power supply stability, PV systems are typically integrated with battery storage [5]. Despite their widespread use, batteries face limitations such as reduced cycle life under frequent cycling, slow dynamic response, and sensitivity to charging irregularities [6]. Supercapacitors, characterized by high power density and rapid charge-discharge capability, present a viable complementary solution. While batteries respond on the order of seconds, supercapacitors operate in the millisecond range, making them effective in mitigating short-term power fluctuations. Based on these characteristics, this paper proposes the implementation of a Hybrid Energy Storage System (HESS), combining batteries and supercapacitors to improve voltage stability and dynamic performance in standalone PV applications under variable irradiance conditions [7]. Based on the energy storage system (ESS) configuration implemented in the off-grid PV system, it is essential to adopt an energy management strategy (EMS) capable of performing maximum power point tracking (MPPT), coordinating power allocation between the battery and the supercapacitor, and maintaining power equilibrium between the generation and load sides.

In this paper, an EMS is developed to regulate power distribution between the PV source and the ESS components, to maintain energy balance and ensure voltage stability at the DC bus. Within the proposed control scheme, the supercapacitor is designated to handle rapid load transients, while the battery is responsible for compensating gradual power variations. Additionally, battery charging is controlled based on the maximum state of charge (SOC) threshold to prevent degradation and extend battery lifespan. System validation is carried out through simulations in MATLAB/Simulink under varying load and irradiance conditions. To further support the findings, additional testing is conducted using a commercial load and real-time irradiance data. The results demonstrate that the proposed strategy is effective in meeting dynamic load demands, preserving system stability, and preventing battery overcharge.

2. Literature Study

2.1 Photovoltaic System

2.1.1 Irradiance

Solar energy generates electricity through two topologies: PV and thermal systems. The terminology PV comes from the light emitted from the sun (photo) to generate a DC voltage (voltaic). Electrical power is generated when exposing PV cells to solar irradiance, causing the electrons to move around, starting an electric current. The

peak solar irradiance on a sunny day is 1000 W/m^2, which is called "one sun" or "peak sun". When the solar irradiance is less than one sun, it will reduce the output current of the PV array proportionally. To get the maximum output from the PV module, it must be pointed directly at the sun [8]. Fig 1 illustrates the I-V and P-V characteristics of a PV module for variation of the sun's irradiation.

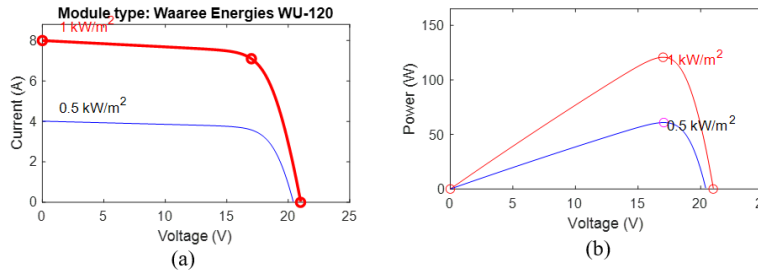

Figure 1. (a) I-V and (b) P-V characteristic of a PV module for variation of the sun's irradiation

The PV module's temperature affects the output voltage inversely. Higher temperature reduces the output voltage of the PV module. At high temperatures, the output voltage will fall by 0.04 to 0.1 volts for every 1 ∘ C rise in temperature. To avoid the rise in temperature, air should be circulated behind the back of each PV module.

2.1.2 Maximum Power Point Tracking

Maximum power point tracking (MPPT) is a technique used in solar panels with the aim of maximizing input power under any conditions. For MPPT, the structure of the solar panel remains generally, and uses a controller containing an algorithm, and uses a DC-DC converter to obtain maximum and efficient power [9]. The current characteristic image based on irradiation shows the working system of the solar panel that works when receiving solar irradiation and obtaining power with the formula P = V.I

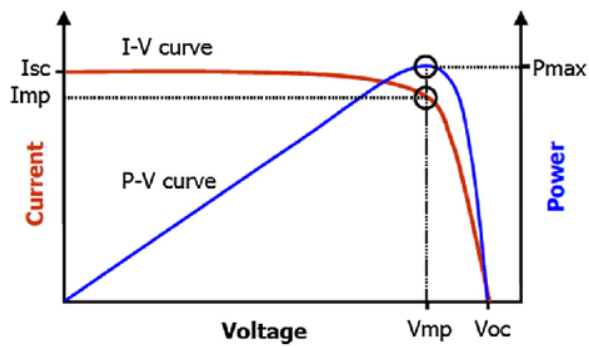

Figure 2. I-V and P-V Curve for maximum power point profile

In the I-V and P-V MPP turtle image, there is a point at the maximum peak of I-V and P-V, resulting in: Vmpp, Impp, Pmpp, as illustrated in Fig 2. The Impp value is the maximum peak current where the condition in I is accompanied by the voltage value (Vmpp). If the Impp and Vmpp values are multiplied, the maximum power will be met in the performance of the solar cell. The maximum power current will be smaller in value compared to the short circuit current value (Isc). This is what is meant by maximum power point [10].

2.1.3 Perturb and Observe

This method works by perturbing (increasing or decreasing) the duty cycle. Every time the duty cycle changes, the power changes will be seen. If the current power is greater than the previous power, the duty cycle will be increased again. If the current power is smaller than the previous power, the duty cycle will be reduced. Therefore, this method requires input of the output power value to determine the power that falls on the load. P&O is also called the hill climbing method, which refers to the V-P characteristics of the PV cell. 3 types of points are in 3 positions to the left of the peak, $dP/dV>0$, at the peak of the $dP/dV=0$ curve, and to the right of the peak, $dP/dV<0$ as shown in Fig 3 [11].

2.2 Converter

2.2.1 Boost Converter

A boost converter is used to control the solar PV power. Fig 4 shows a simplified schematic of the boost converter. Inductor L and capacitor C make up the effective output filter. The capacitor equivalent series resistance (ESR), RC, and the inductor DC resistance, RL, are included in the analysis. Resistor R represents the load seen by the power supply output [12].

The inductor functions as the magnetic energy storage component, where energy is stored within its core material. The switching operation is controlled by the PWM signal, while the transistor serves as the switching element. The diode and capacitor are utilized to perform the roles of rectification and filtering in the output stage of the circuit [13]. The value of the boost converter inductor is

$$L = \frac{D.Vin}{f\Delta i} \tag{1}$$

L : Inductance (H)
D : Duty Cycle
Vin : Input Voltage (V)
F : Frequency (Hz)
Δi : Ripple Current
The value of the boost converter capacitor is

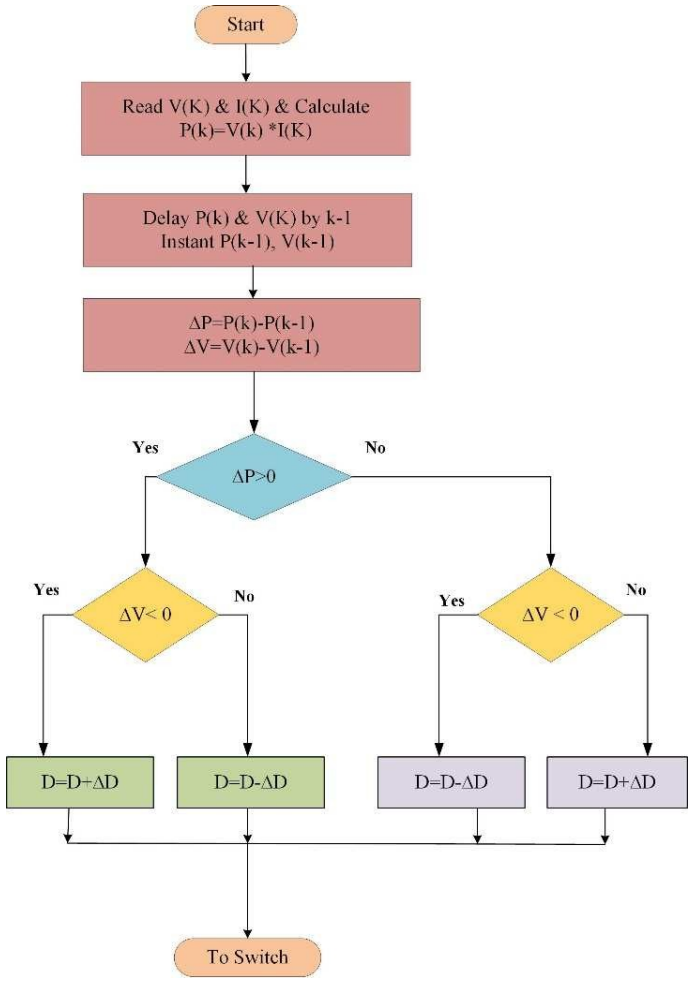

Figure 3. Perturb and Observe MPPT algorithm

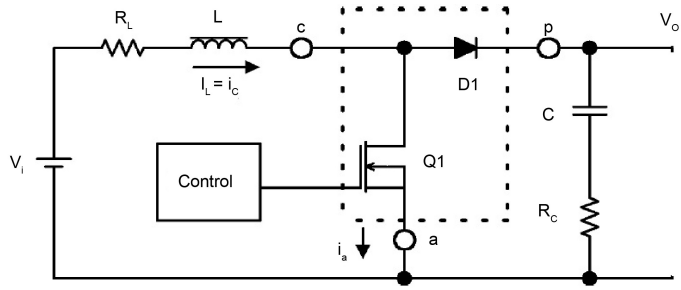

Figure 4. Boost DC/DC Schematic

$$C = \frac{D.Vout}{f.R\Delta v} \tag{2}$$

L : Inductance (H)
D : Duty Cycle
Vout : Output Voltage (V)
F : Switching Frequency (Hz)
Δv : Ripple Voltage

Where D is the duty cycle, Vin and Vout are the voltage output and input of the boost converter, and f is the switching frequency, Δi (10% of Iomax) and Δv (0.02% to 0.05% of Vo) is ripple current and ripple voltage.

2.2.2 Bidirectional Converter

Fig 5 shows the basic structure of a buck-boost converter, along with the modification required to transform it into a bidirectional converter by replacing the diode within the circuit [13].

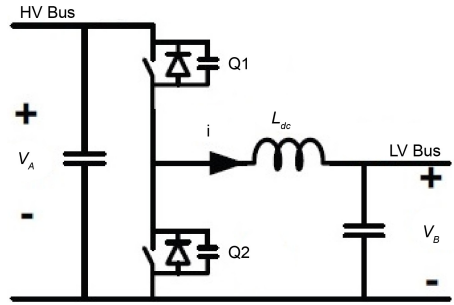

Figure 5. Bidirectional buck boost converter circuit

The value of the boost converter inductor is

$$L = \frac{D.Vin.Ts}{\Delta iL} \tag{3}$$

Where Ts is the switching period L : Inductance (H) D : Duty Cycle Vin : Input Voltage (V) F : Frequency (Hz) Δi : Ripple Current Ts : Switching Period

2.3 Hybrid Energy Storage System

The comparison structure of a battery and supercapacitor is presented in Fig 6. Furthermore, a supercapacitor offers advantage of high power density, while the battery excels in high energy density. A hybrid system that combines both components integrates the advantages of each[14][15][16] [17].

The lithium-ion battery working principle is given in Fig 6 (a) [18]. Li-ion cells consist of two electrodes, the anode and cathode. Graphite is used as an anode, and the lithium metal oxide is used as a cathode. The lithium salt in an organic solvent

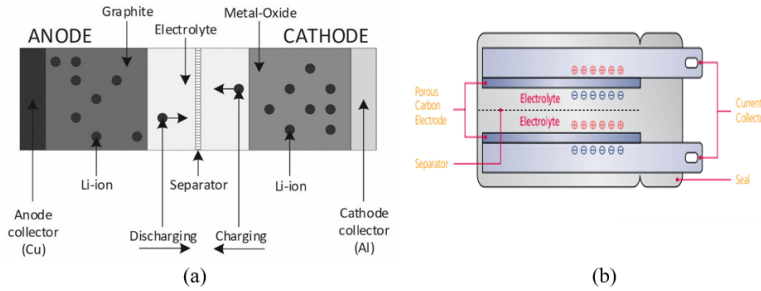

Figure 6. (a) Battery structure and (b) Supercapacitor structure

is used as an electrolyte. The anode collector is made of copper (Cu) and cathode collector is made of aluminum (Al). The working principle of this technology is based on Li-ions moving from the cathode to the anode when the battery is in the charging process and from the anode to the cathode when the battery is in the discharging process [19].

Fig 6 (b) illustrates the construction of a supercapacitor [20]. A supercapacitor is an electrical energy storage device characterized by its high power density, which was previously difficult to achieve with conventional capacitors. It consists of two electrodes immersed in an electrolyte solution, separated by a membrane that prevent the transfer of electric charge between the two oppositely polarized electrodes.

3. Research Methods

3.1 PV + HESS Configuration

Figure 7. PV + HESS Configuration

The configuration of solar energy storage using a hybrid energy storage system is illustrated in Fig. 7, which consists of a PV panel, a boost converter with a Perturb and Observe (P&O) MPPT algorithm, and two energy storage units: a supercapacitor and a battery.

3.2 Battery Specification

The specification of the battery to be used is shown in Table 1.

Table 1. Li-Ion battery specification

Parameter	Value	Unit
Nominal Voltage	24	V
Rated Capacity	14	Ah
State of Charge	90 and 97	%

3.3 PV Specification

The specification of the PV array to be used is shown in Table 2.

Table 2. PV array specification

Parameter	Value	Unit
Maximum Power	120.7	W/m^2
Open Circuit Voltage	21	V
Short Circuit Current	8	A
Voltage at the maximum power point	17	V
Current at the maximum power point	7.1	A

3.4 Supercapacitor Specification

The specification of the supercapacitor to be used is shown in Table 3.

Table 3. Supercapacitor Specification

Parameter	Value	Unit
Rated Voltage	32	V
Rated Capacitance	29	F

3.5 Boost Converter Specification

The specification of the boost converter to be used is shown in Table 4.

3.6 Bidirectional Converter Specification

The specification of the low-pass filter (LC filter) to be used is shown in Table 5.

3.7 Irradiation and Load Profile

The load and irradiance profiles used in this study correspond to the characteristics of a commercial office load as shown in Table 6, Fig. 8, and Fig. 9. The office operates from 8:00 AM to 5:00 PM.

Table 4. Boost converter specification

Parameter	Value	Unit
Vin	40	V
Vout	50	V
Iin	26	A
ΔVc (ripple arus)	17.5	%
ΔIL (ripple tegangan)	0.76	%
Frekuensi switching	5000	Hz
Duty cycle	0.2	
Inductor	0.000352	Hz
Capacitor	0.0022	F

Table 5. Bidirectional Converter Specification

Parameter	Value	Unit
Inductor	0.000355	H
Capacitor	0.0003	F

Table 6. Irradiation and Load Profile

Hours	Load(W)	Jan-Jul (W/m^2)	Load(W)	Aug-Dec(W/mV^2)
8 a.m.	566	340	366	100
9 a.m.	566	500	366	200
10 a.m.	566	660	366	350
11 a.m.	566	840	366	500
12 p.m.	566	1000	366	620
1 p.m.	657	1100	385	620
2 p.m.	446	900	400	600
3 p.m.	446	800	400	460
4 p.m.	532	700	332	300
5 p.m.	532	500	332	120
6 p.m.	56	400	56	50

3.8 Control Strategy

3.8.1 MPPT for PV

To enable PV to deliver maximum power, a maximum power point tracker (MPPT) is used to find and maintain the PV's maximum power. An MPPT algorithm controls the boost converter to extract the maximum power from the PV under varying weather conditions. The algorithm employed is Perturb and Observe (P&O) as shown in Fig 10. The inputs to the algorithm are the voltage (V) and current (I) from the PV, which are used to calculate the PV power (P). When both PV power and voltage increase, the algorithm increases the duty cycle (ΔD). The duty cycle (D) is incremented by a

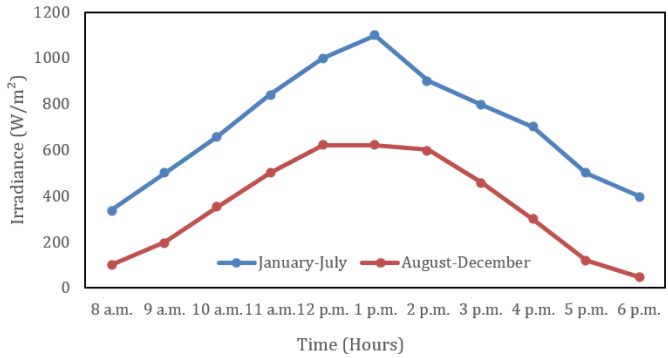

Figure 8. Irradiation Data in January-December

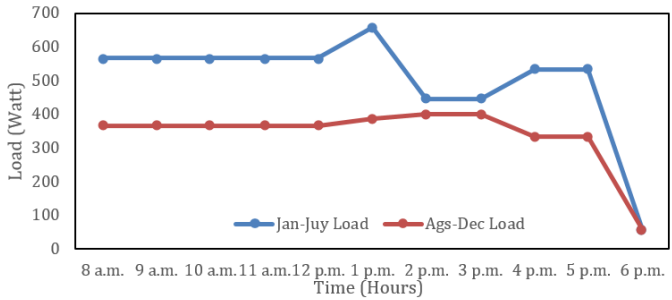

Figure 9. Load Data in January-December

predefined step size to adjust the operating point toward the maximum power point (MPP), and likewise in the reverse direction when the power decreases.

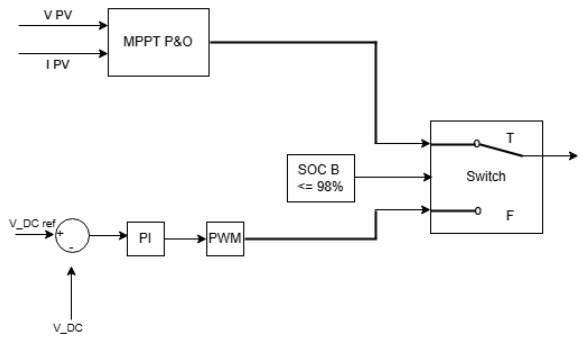

Figure 10. MPPT Control

When the power from the PV (P_{PV}) is greater than the load power (P_{load}), the excess power from the PV will be distributed to the battery, even though the battery is full, which can cause battery degradation. Therefore, as shown in Figure 3.5 when

the battery SOC is >= 98%, the MPPT will be disabled and the PV will only supply enough power to maintain a stable DC voltage (V_{DC}), without involving the battery

3.8.2 Hybrid Energy Storage Control

As previously discussed, the supercapacitor (*SC*) is primarily added to absorb short-term energy surges caused by fluctuations in weather conditions that affect the PV output power, with the aim of reducing the charging burden on the battery. To achieve this functionality, the power difference between the generation side and the consumption side is divided into two components: a low-frequency component (*LFC*) representing stable variations, and a high-frequency component (HFC) representing transient fluctuations. The battery is responsible for managing the former, while the SC compensates for the latter. The PI parameters for the HESS voltage control loop are P = 1.472, I = 3072. The PI parameters of the supercapacitor current controller loop and battery current controller loop is P_{SC} = 0.043, I_{SC} = 0.65, and P_B = 0.45, I_B = 14.800, respectively.

The control scheme illustrated in Fig. 11 implements a strategy in which the battery is responsible for handling slow transients, while the supercapacitor manages fast transients. The DC voltage (V_{DC}) is compared to the reference voltage (V_{DCref}) and processed through a PI controller, resulting in a reference current value ($I_{totalref}$). This current is then divided into two parts: the low-frequency power component and the high-frequency power component, using a low-pass filter (LPF). The output of the LPF represents the average or low-frequency current, which serves as the reference current for the battery (I_{bref}). I_{bref} is then compared with the actual battery current (I_{batt}), and the resulting error is fed into another PI controller. The controller output is passed through a PWM block to generate the appropriate switching signals for either Q1 or Q2. $I_{scnewref}$ is compared with the actual supercapacitor current (I_{sc}), and the resulting error is fed into a PI controller. The output of the controller is then passed through a PWM block to generate the appropriate switching signals for either Q1 or Q2.

$$I_{totalref} = V_{DCref} - V_{DC} \tag{4}$$

$$I_{bat\_ref} = (LPF)I_{totalref} \tag{5}$$

$$I_{bat\_newref} = I_{bat\_actual} \tag{6}$$

Due to the slower dynamic response of the battery compared to the supercapacitor, the actual battery current is unable to accurately follow the reference current during rapid changes in load or power supply. As a result, a portion of the power remains uncompensated by the battery, as described below:

$$Pb_{bat\_uncomp} = (I_{batt\_ref} - I_{batt\_actual}) * V_{bat} \tag{7}$$

The uncompensated power is compensated by the supercapacitor. So, the new reference current of the supercapacitor is given by Eq. (10).

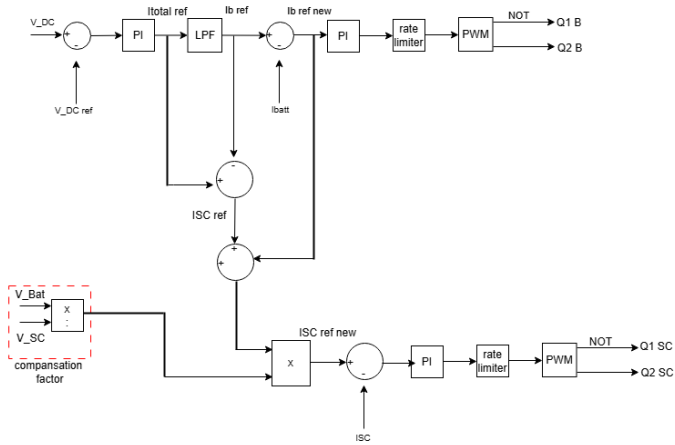

Figure 11. HESS Control Strategy

$$I_{totalref} - I_{batt\_reff} = I_{sc\_ref} \tag{8}$$

$$I_{SC\_ref} + (I_{bat\_ref} - I_{bat\_actual}) \times \frac{V_{bat}}{V_{SC}} = I_{sc\_newref} \tag{9}$$

$$I_{sc\_newref} = I_{totalref} - I_{batt\_ref} + (I_{bat\_ref} - I_{bat\_actual}) \times \frac{V_b}{V_{SC}} \tag{10}$$

With the proposed control scheme employing a compensation factor (CF), the energy that cannot be supplied by the battery will be fulfilled by the supercapacitor when there is a change in irradiation that affects the PV output power, which also affects the fulfillment of power to the load. This can accelerate the DC voltage to follow the reference voltage. In addition, the supercapacitor also supplies temporary power until the battery reaches a stable power discharge so that it can improve battery performance and life. Once the system reaches steady-state conditions, the uncompensated power becomes minimal and has an insignificant impact on overall system operation.

4. Results and Discussion

Fig. 12 illustrates the configuration of a hybrid energy storage system consisting of a photovoltaic panel, a boost converter equipped with a Perturb and Observe (*P&O*) MPPT algorithm, and two energy storage units: a supercapacitor and a battery. Both storage elements are connected to the system through bidirectional converters, which are controlled using the control scheme described in Chapter 3. The supercapacitor is responsible for providing a fast response to short-term power fluctuations, while the battery supplies energy over longer durations. This system is designed to maintain DC voltage stability despite load variations or changes in solar panel output caused by fluctuations in irradiance.

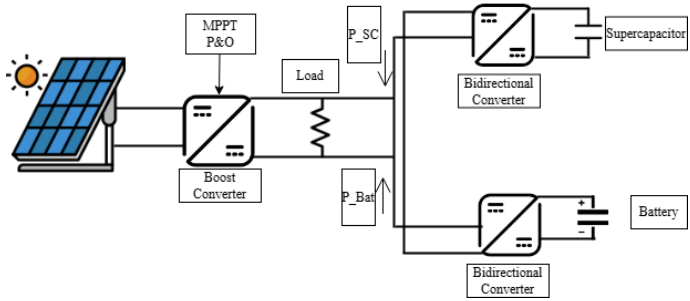

Figure 12. PV + HESS Configuration

Table 7. Caption

Studied Cases	Parameters		Decision	
	Jan-Jul	Aug-Dec	Jan-Jul	Aug-Dec
t=0 - 1 s	Irr = 340 W/m^2 Load = 566 W Batt SOC >98%	Irr = 100 W/m^2 Load = 366 w Batt SOC >98%	PPV = 327 W PLoad = 566 W PBat = 291 W (disch) PLosses = 52 W	PPV = 93 W PLoad = 366 W PBat = 284 W (disch) PLosses = 11 W
t=1 - 2 s	Irr = 500 W/m^2 Load = 566 W Batt SOC >98%	Irr = 200 W/m^2 Load = 366 W Batt SOC >98%	PPV = 485 W PLoad = 566 W PBat = 128 W (disch) PLosses = 47 W	PPV = 189 W PLoad = 366 PBat = 235 W (disch) PLosses = 58 W
t=2 - 3 s	Irr = 660 W/m^2 Load = 566 W Batt SOC >98%	Irr = 350 W/m^2 Load = 366 Batt SOC >98%	PPV = 640 W PLoad = 566 W PBat = -25 W (charge) PLosses = 49 W	PPV = 337 W PLoad = 366 W PBat = 81 W (disch) PLosses = 52 W
t=3 - 4 s	Irr = 840 W/m^2 Load = 566 W Batt SOC >98%	Irr = 500 W/m^2 Load = 366 W Batt SOC >98%	PPV = 813 W PLoad = 566 W PBat = -188 W (charge) PLosses = 59 W	PPV = 484 W PLoad = 366 W PBat = -65 W (charge) PLosses = 53 W
t=4 - 5 s	Irr = 1000 W/m^2 Load = 566 W Batt SOC >98%	Irr = 620 W/m^2 Load = 366 W Batt SOC >98%	PPV = 965 W PLoad = 566 W PBat = -328 W (charge) PLosses = 71 W	PPV = 601 W PLoad = 366 W PBat = -177 W (charge) PLosses = 58 W
t=5 - 6 s	Irr = 1100 W/m^2 Load = 657 W Batt SOC >98%	Irr = 620 W/m^2 Load = 385 W Batt SOC >98%	PPV = 1057 W Load = 657 W PBat = -327 W (charge) PLosses = 73 W	PPV = 601 W Load = 385 W PBat = -150 W (charge) PLosses = 66 W
t=6 - 7 s	Irr = 900 W/m^2 Load = 446 W Batt SOC >98%	Irr = 620 W/m^2 Load = 400 W Batt SOC >98%	PPV = 871 W PLoad = 446 W PBat = -356 W PLosses = 69 W	PPV = 582 W PLoad = 400 W PBat = -130 W (charge) PLosses = 52 W

Studied Cases	Parameters		Decision	
	Jan-Jul	Aug-Dec	Jan-Jul	Aug-Dec
t=7 - 8 s	Irr = 800 W/m^2 Load = 446 W Batt SOC >98/%	Irr = 460 W/m^2 Load = 400 W Batt SOC >98%	PPV = 765 W PLoad = 446 W PBat = -266 W (charge) PLosses = 53 W	PPV = 445 W PLoad = 400 W PBat = 50 W (disch) PLosses = 95 W
t=8 - 9 s	Irr = 700 W/m^2 Load = 532 W Batt SOC >98%	Irr = 300 W/m^2 Load = 332 W Batt SOC >98%	PPV = 679 W PLoad = 532 W PBat = -85 W (charge) PLosses = 62 W	PPV = 287 W PLoad = 332 W PBat = 96 W (disch) PLosses = 51 W
t=9 - 10 s	Irr = 500 W/m^2 Load = 532 W Batt SOC >98%	Irr = 120 W/m^2 Load = 332 W Batt SOC >98%	PPV = 484 W PLoad = 532 W PBat = 102 W (disch) PLosses = 54 W	PPV = 112 W PLoad = 332 W PBat = 242 W (disch) PLosses = 22 W
t=10 -11 s	Irr = 400 W/m^2 Load = 56 W Batt SOC >98%	Irr = 50 W/m^2 Load = 56 W Batt SOC >98%	PPV = 382 W PLoad = 56 W PBat = -165 W (charge) PLosses = 161 W	PPV = 45 W PLoad = 56 W PBat = 15 W (disch) PLosses = 4 W

To verify the performance of the proposed system and the validity of the implemented controls, the considered system is tested using MATLAB/Simulink for the case study in Table 7.

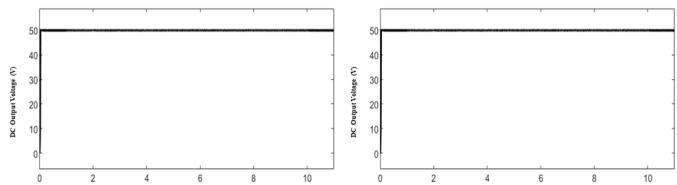

Figure 13. DC bus voltage during simulation with CF, (a) Jan-Jul and (b) Aug-Dec

Fig. 13 shows that the DC link voltage is successfully regulated at 50V according to the voltage reference. Whereas Fig. 14 shows that the DC link voltage varies and has some fluctuation during the transient period throughout the simulation period.

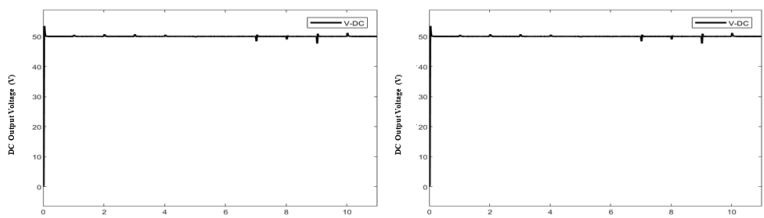

Figure 14. DC Bus Voltage During Simulation without CF, (a) Jan-Jul and (b) Aug-Dec

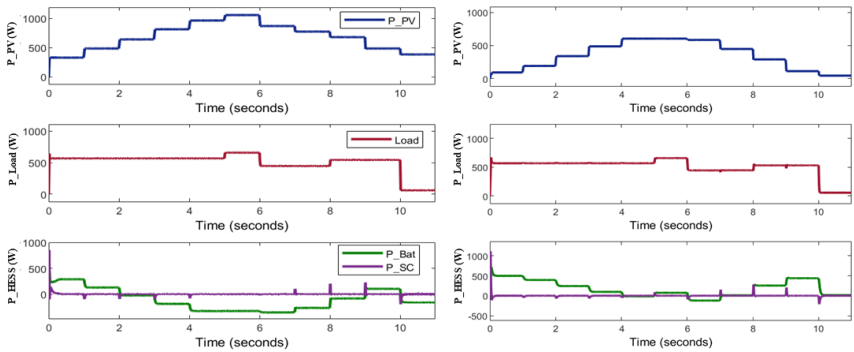

Figure 15. Simulation Result of Power Sharing in PV and HESS with CF, (a) January-July, (b) August-December

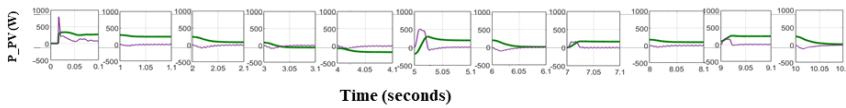

Figure 16. Simulation results of power sharing in PV and HESS with CF at several zoomed time intervals

Fig. 15 shows the power required by the load and produced by the PV and HESS. Fig. 16 shows the power required by the load and the PV and HESS output power. In Fig. 15(a), it is shown that the maximum PV power is accurately tracked according to the irradiance around the PV array, and also shows the load change from 366 to 385W at t=5-6 seconds. During the period (3 < t < 9s), the battery does not operate to supply the load because the output power from the PV is sufficient to meet the load demand. In this interval, the battery is in charging mode. Fig. 15 (b) shows that the maximum PV power is also accurately tracked according to the irradiance around the PV array, and also shows the load change from 385 to 400W at t=5-8 seconds. During the period (3 < t < 8s), the battery does not operate to supply the load because the output power from the PV is sufficient to meet the load demand. In this interval, the battery is in charging mode. By analyzing the constant power values generated from PV, Load, and battery, which are presented in Table 7 and Fig 15(a) and (b) for each case, it is evident that the required energy balance is guaranteed and the load is always met.

Fig. 16 shows the transient power response of the HESS at several zoomed time intervals. It can be observed that during each power variation, the supercapacitor exhibits very fast power spikes, particularly within the time range of t = (0 > t >9s), indicating its capability to handle rapid power fluctuations. In contrast, the battery response appears smoother and more gradual, demonstrating its role in compensating for more stable and slower power variations. Fig. 17 shows the power required by the load and the PV and HESS output power with CF.

Fig. 17 shows the simulation results comparing the HESS performance with and without the compensation factor. In Fig. 17(a), under the with compensation factor

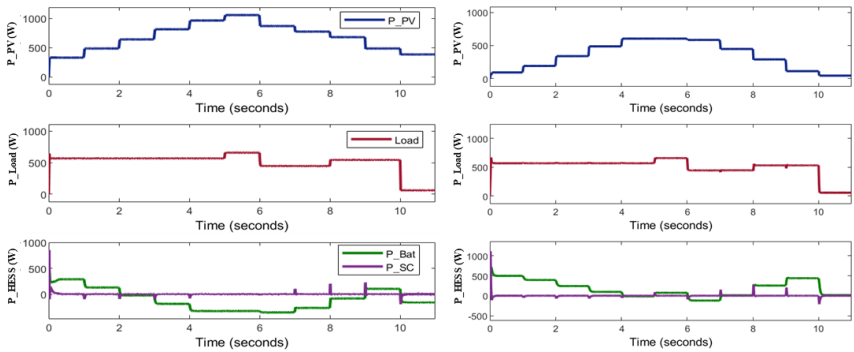

Figure 17. Simulation Result of Power Sharing in PV and HESS in January - July, (a) With CF, (b) Without CF

condition, the PV power increases gradually and reaches its maximum value of 964W at 6s, while the load demand is 657 W. Therefore, the excess power generated by the PV is utilized to charge the battery with approximately 327 W. During the 5–6 s interval, when the PV power begins to decrease, the HESS provides coordinated power compensation to maintain system stability.

In contrast, Fig. 17(b), representing the condition without the compensation factor, shows that the PV output does not reach the expected maximum value at each time step. For example, at t = 6 s, the PV power is only 599 W, while the load demand remains 657 W. Under normal conditions, this load demand should be supplied by the PV output, while the remaining power is used for battery charging when the compensation factor is applied. Therefore, without the compensation factor, the HESS fails to provide coordinated power compensation, resulting in less optimal power sharing performance.

Fig. 18 shows the power required by the load and the PV and HESS output power with and without CF, and Fig. 19 shows the voltage across, the current through, and the SOC of the battery with and without CF.

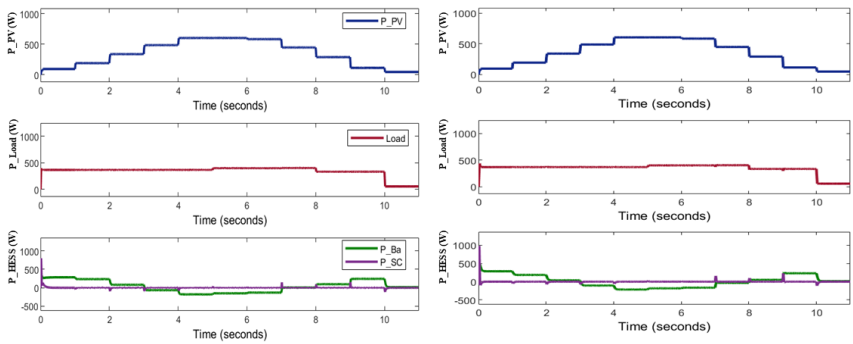

Figure 18. Simulation Result of Power Sharing in PV and HESS August - December, (a) With CF, (b) Without CF

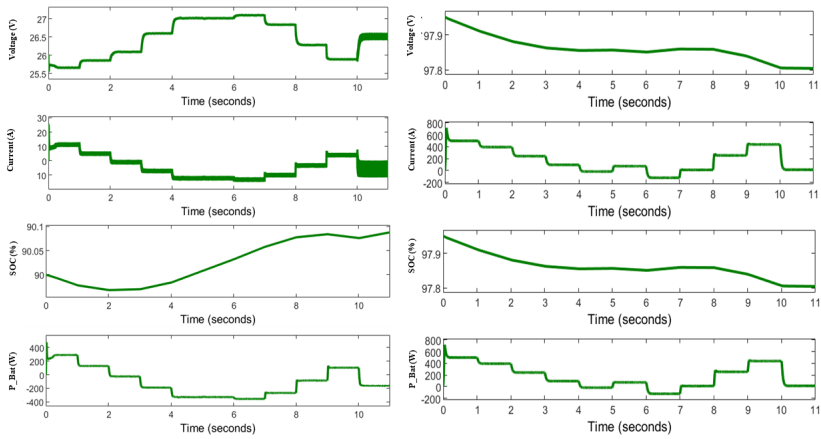

Figure 19. Simulation Result of Battery Voltage, Current and SOC in August-December, (a) With CF, (b) Without CF

Based on Figure 19 (a), the application of the compensation factor (CF) provides a more stable battery response compared to the case without CF. During the interval t = 0–4 s, the battery voltage increases gradually, indicating the charging process, while the current varies smoothly without significant fluctuations. In addition, the battery SOC exhibits a smoother profile, suggesting a reduced frequency of charge–discharge cycles. In contrast, as shown in Figure 19(b), the condition without CF presents more abrupt changes in current and power within the interval t = 6–9 s, indicating increased operational stress on the battery

The battery current will be positive if it is in the charging mode, and the voltage and SOC will increase, and vice versa, the battery current will be negative if it is in the discharging mode, and the voltage and SOC will decrease.

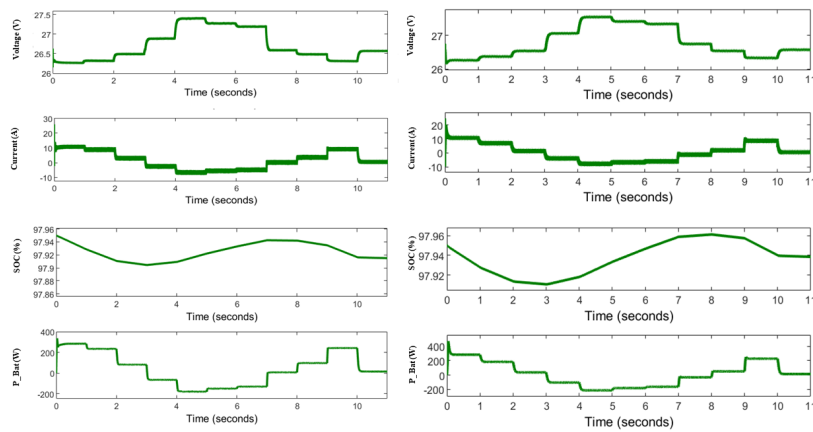

Figure 20. Simulation Result of Battery Voltage, Current and SOC, in August-December (a) With CF, (b) Without CF

In Figure 20 (a), the use of the compensation factor produces a more stable battery profile compared to the condition without the compensation factor shown in Figure 20(b). During the interval t = 0–3 s, the battery undergoes a discharging process, as indicated by the gradual change in voltage and the decrease in SOC from 97.94% to 97.90%

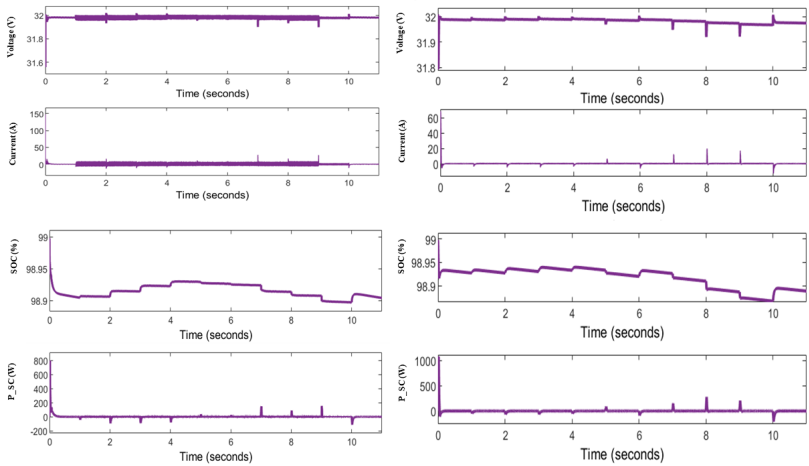

Figure 21. Simulation Result of Supercapacitor Voltage, Current and SOC in January - July, (a) With CF, (b) Without CF

In Fig. 21 (a) the current and voltage of the supercapacitor tend to remain relatively stable throughout the simulation due to its limited energy storage capacity. Nonetheless, its rapid dynamic response allows it to absorb and release energy over very short time intervals, causing changes in current and voltage to be less noticeable. In contrast, the state of charge (SOC) exhibits fluctuations resulting from continuous charging and discharging events during the simulation period.

In Figure 22 (a), which applies the compensation factor, the supercapacitor voltage remains relatively more stable throughout the simulation compared to Figure 22 (b) without the compensation factor. This indicates that, without the compensation factor, the supercapacitor response to power variations is lower and less effective. In addition, the current profile shows significant spikes within the interval t = 6–9 s. These current surges indicate that the supercapacitor actively responds to rapid power changes, demonstrating its ability to compensate for fast transient power fluctuations

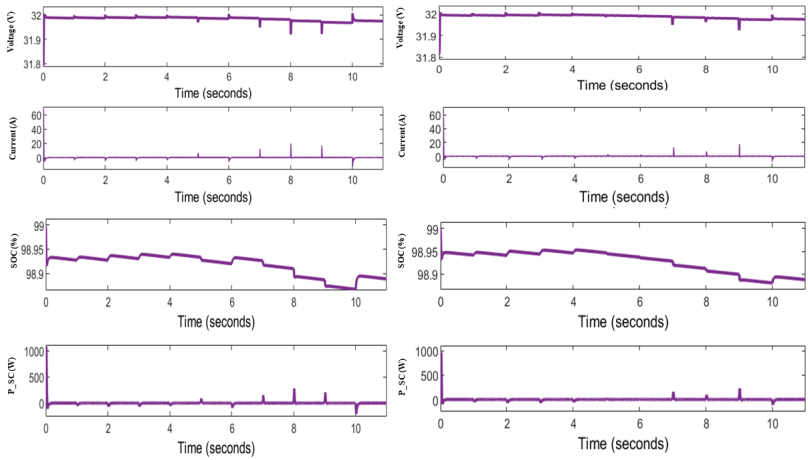

Figure 22. Simulation Result of Supercapacitor Voltage, Current and SOC in August – December, (a) With CF, (b) Without CF

5. Conclusion

This paper presents a comparison between the HESS control strategy with and without the compensation factor under various PV generation and load demand conditions. The results show that the use of the compensation factor enables the DC output voltage to reach its reference value more rapidly compared to the case without the compensation factor. This improvement is achieved through better coordination between the battery and the supercapacitor, where the supercapacitor effectively compensates for high-frequency power fluctuations while the battery provides stable low-frequency power support. Consequently, battery stress is reduced, which can contribute to improved battery performance and longer service life. Furthermore, the proposed method is simple to implement and may be further enhanced through optimal sizing and parameter tuning of the battery and supercapacitor units.

References

[1] Y. Alhorr, E. Eliskandarani, and E. Elsarrag. "Approaches to Reducing Carbon Dioxide Emissions in the Built Environment: Low Carbon Cities". In: *International Journal of Sustainable Built Environment* 3.2 (2014), pp. 167–178. DOI: 10.1016/j.ijsbe.2014.11.003.

[2] G. R. Timilsina and A. Shrestha. "Transport Sector CO2 Emissions Growth in Asia: Underlying Factors and Policy Options". In: *Energy Policy* 37.11 (2009), pp. 4523–4539. DOI: 10.1016/j.enpol.2009.06.009.

[3] A. Wijaya et al. *How Can Indonesia Achieve Its Climate Change Mitigation Goal?* Tech. rep. Online. World Resources Institute, 2017. URL: https://wri-indonesia.org/sites/default/files/WRI%20Layout%20Paper%20OCN%20v7.pdf.

[4] R. Susanto, W. Lestari, and H. Hasanah. "Performance Analysis of Solar Panels in Tropical Region: A Case Study in Surakarta Indonesia". In: *International Conference on Science, Health and Technology*. 2022, pp. 1–13. DOI: 10.47701/icohetech.v3i1.2059.

[5] H. B. Nurjaman and T. Purnama. "Pembangkit Listrik Tenaga Surya (PLTS) Sebagai Solusi Energi Terbarukan Rumah Tangga". In: *Jurnal Edukasi Elektro* 6.2 (2022), pp. 136–142. DOI: 10.21831/jee.v6i2.51617.

[6] K. M. Moloelang et al. "Modeling and Analysis of a Battery-Supercapacitor Hybrid Energy Storage System (HESS)". In: *6th International Conference on Renewable Energy and Power Engineering (REPE)*. 2023, pp. 293–299. DOI: 10.1109/REPE59476.2023.10511902.

[7] O. Saadeh, S. Al Tamimi, and F. Amoura. "A Hybrid Battery/Ultracapacitor Energy Storage Solution for PV Systems". In: *IEEE International Energy Conference*. 2020, pp. 384–388. DOI: 10.1109/ENERGYCon48941.2020.9236532.

[8] S. S. Panagoda et al. "Advancements in Photovoltaic Technology for Solar Energy Generation". In: *Journal of Research in Technology and Engineering* 4.3 (2023). Online, pp. 30–72.

[9] R. Amirillah et al. "Rancang Bangun Sistem Pompa Aerator Tenaga Surya". In: – (2023), pp. 31–32.

[10] S. Ahmad. "Solar Cell Under Variable Temperature and Insolation Using LabVIEW Based Simulator". In: – 8.9 (2020), pp. 2095–2098.

[11] S. C. Wang et al. "A Fast and Efficient Maximum Power Tracking". In: *IEEE Access* 8 (2020), pp. 155319–155328. DOI: 10.1109/ACCESS.2020.3019197.

[12] H. Kaushik and B. Bhushan. "Performance Analysis of Boost Converters in a PV System". In: *IEEE Delhi Section Conference*. 2022, pp. 1–7. DOI: 10.1109/DELCON54057.2022.9752878.

[13] A. Thiyagarajan, S. G. Praveen Kumar, and A. Nandini. "Analysis and Comparison of DC/DC Boost Converter". In: *ICCTET*. 2014, pp. 198–205. DOI: 10.1109/ICCTET.2014.6966287.

[14] S. Mallika and R. Saravana Kumar. "Review on Ultracapacitor-Battery Interface". In: *International Journal of Engineering and Technology* 3.1 (2011), pp. 37–43.

[15] A. Du Pasquier et al. "Comparative Study of Li-ion Battery and Supercapacitor". In: *Journal of Power Sources* 115.1 (2003), pp. 171–178. DOI: 10.1016/S0378-7753(02)00718-8.

[16] J. C. Ellenbogen. *Supercapacitors: A Brief Overview*. Tech. rep. 2006.

[17] K. A. Khan and M. Khalid. "Hybrid Energy Storage System for Voltage Stability". In: *IEEE ISGT Asia*. 2019, pp. 2760–2765. DOI: 10.1109/ISGT-Asia.2019.8881611.

[18] H. C. Hesse et al. "Lithium-ion Battery Storage for the Grid". In: *Energies* 10.12 (2017). DOI: 10.3390/en10122107.

[19] Z. Šimić et al. "Battery Energy Storage Technologies Overview". In: *IJECES* 12.1 (2021), pp. 53–65. DOI: 10.32985/IJECES.12.1.6.

[20] LSMtron. *LS Ultracapacitor Brochure*. 2014. URL: http://www.ultracapacitor.co.kr/support/manuals-and-user-guidelines.html.